**Supplementary Fig. 1: Canonical Notch signaling induces prostate epithelial proliferation.**
(a) Transillumination images of urogenital organs of NICD^{WT}, PB-NICD and PB-NICD-Rbp-J$^{fl/fl}$ mice. (b) Prostate weights and prostate cell numbers of NICD^{WT} and PB-NICD

mice at 14, 26, and 52 weeks of age. Data represent means ± s.d. from 3 mice per group. **(c)** H&E staining and IHC analyses of Ki67, cleaved Caspase 3 (CC3) and K8 of NICD^{WT} and PB-NICD mouse prostates. Red arrows point to CC3$^+$ cells. Bar graph shows quantification of Ki67$^+$ cells. Data represent means ± s.d. from 3-5 mice at each time points per group. **(d-e)** qRT-PCR and IHC analysis of AR expression in NICD^{WT} and PB-NICD mouse prostates. Scale bars, 4mm (a); 25μm (c); 50μm (e). Data represent means ± s.d. from 3 pairs of mice. Statistical significance was calculated using the *t*-test (*: $p < 0.05$, **: $p < 0.01$, ***: $p < 0.001$).
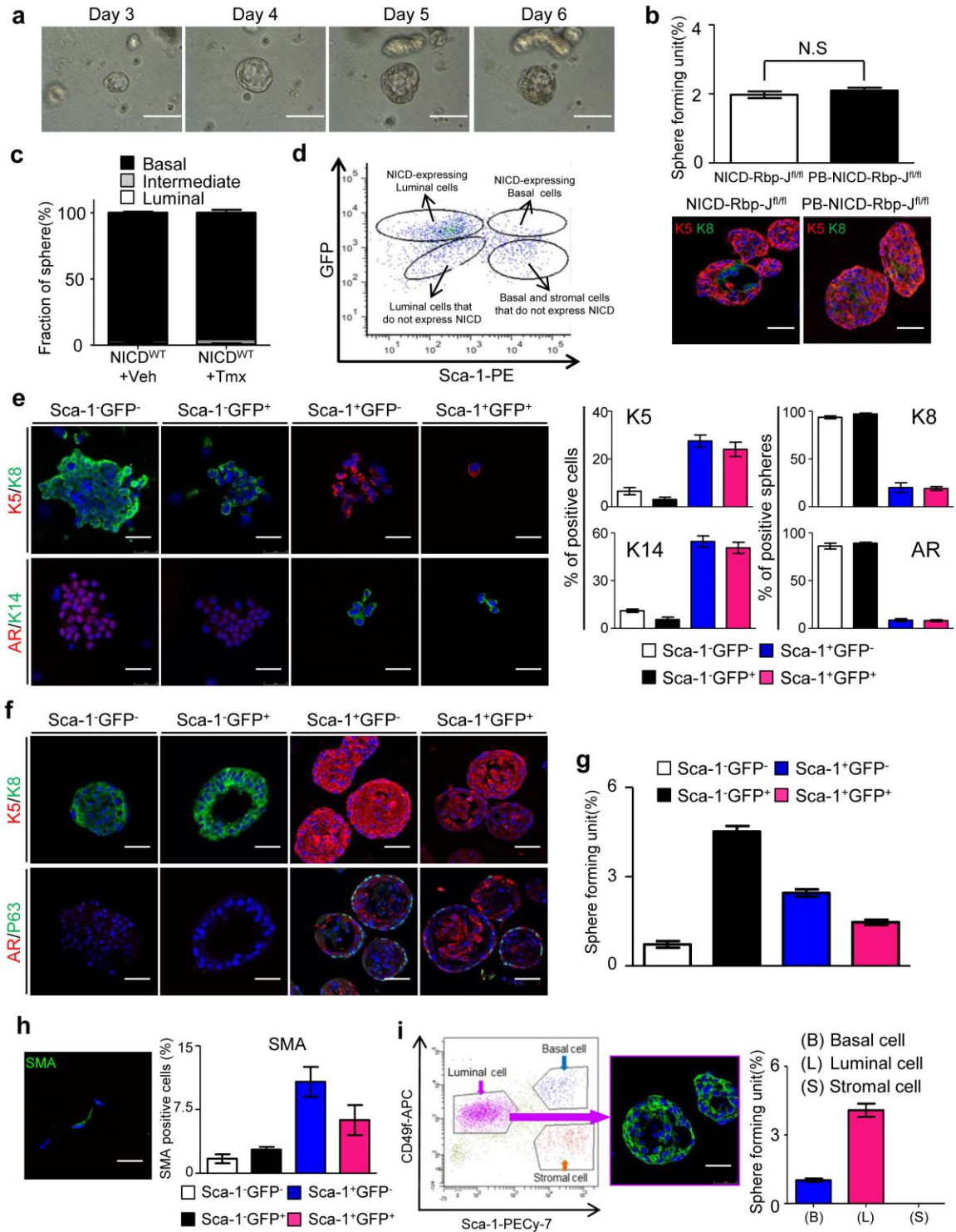
Supplementary Fig. 2: Luminal prostate spheres were generated from NICD-expressing luminal cells in PB-NICD mice.

(a) Time-lapse transillumination images of luminal prostate spheres. **(b)** Formation of luminal spheres is dependent on canonical Notch signaling. Bar graph quantifies sphere-forming units of NICD-Rbp-J$^{fl/fl}$ and PB-NICD-Rbp-J$^{fl/fl}$ prostate cells. Data represent

means ± s.d. from 3 pairs of mice. Images show IHC analyses of K5 and K8 in prostate spheres generated from NICD-Rbp-J$^{fl/fl}$ and PB-NICD-Rbp-J$^{fl/fl}$ mouse prostate cells. (**c**) Tamoxifen treatment does not induce formation of luminal prostate spheres from NICD^{WT} cells. Data represent means ± s.d. from 3 mice per group. (**d**) FACS plot of PB-NICD mouse prostate cells based on Sca-1 and GFP expression. (**e**) Immunocytochemical analyses of K5, K8, K14 and AR on cytospins of the four FACS-sorted populations. Bar graphs on the right show quantifications. Bar graphs in e, g, and h show means ± s.d. from 3 independent experiments. (**f**) Immunhistochemical analyses of K5, K8, P63 and AR in prostate spheres generated from the four FACS-sorted populations. (**g**) Bar graph quantifies the sphere-forming units of the 4 FACS-sorted populations. (**h**) Immunocytochemical analysis of smooth muscle actin (SMA) and bar graph quantification confirm that SMA expression is enriched in Sca-1$^+$ cells that included stromal cells. (**i**) Only FACS-sorted Lin$^-$Sca-1$^-$CD49f^{low} cells in PB-NICD mice generated prostate luminal spheres. Scale bars, 100μm (a); 25μm (b, e, f, h, i). Data represent means ± s.d. from 3 different experiments using 2-4 mice in each experiment.
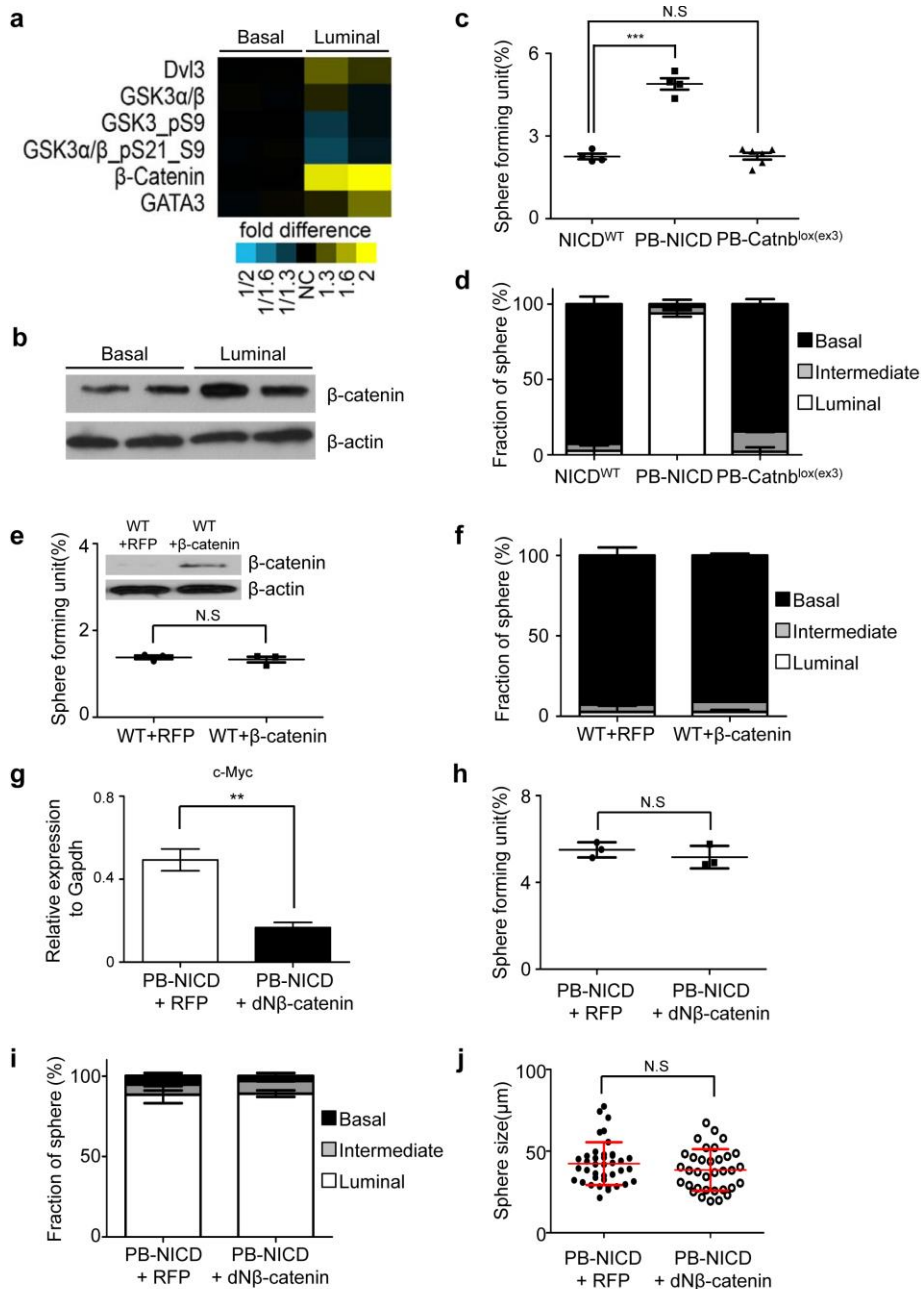
Supplementary Fig. 3: β-catenin transcriptional activity is neither essential nor sufficient for the formation of PB-NICD luminal spheres.
**(a)** Reverse phase protein array shows expression of several Wnt signaling components in basal and luminal prostate spheres cells. **(b)** Western blot analysis of β-catenin in basal and luminal prostate sphere cells. Individual lanes represent independent samples. **(c,d)** Quantification of sphere-forming units and the types of prostate spheres generated from prostate cells of NICD[WT], PB-NICD and PB-Catnb[lox(ex3)] mice . Data represent means ± s.d. from 3 mice per group. **(e,f)** β-catenin is not sufficient to drive the formation of luminal prostate spheres. Dot (e) and bar (f) graphs quantify the sphere-forming units and the types of prostate spheres generated from WT prostate cells that have been infected by RFP lentivirus and β-catenin lentivirus separately. Data represent means ± s.d. from one

of the two independent experiments. Data represent means ± s.d. from 3 independent experiments. **(g)** Ectopic expression of dominant negative β-catenin in PB-NICD luminal prostate cells suppresses c-Myc expression. Data represent means ± s.d. from 3 independent experiments. **(h-j)** β-catenin transcriptional activity is not essential for the formation of luminal prostate spheres. Dot and bar graphs quantify the sphere-forming units (h) and the types of prostate spheres (i) and the size of prostate spheres (j) generated from PB-NICD prostate cells that have been infected by RFP lentivirus and dominant negative β-catenin lentivirus separately. Data represent means ± s.d. from 3 independent experiments. Statistical significance was calculated using the *t*-test (**: p < 0.01, ***: p < 0.001).
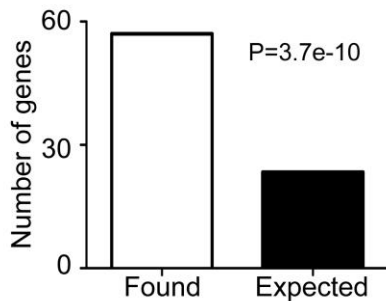

Supplementary Fig. 4: GO analysis shows that gene ontology group related to AKT activity is enriched in PB-NICD mouse prostates as compared to WT mouse prostates.
Genes up-regulated by AKT in mouse model of prostate cancer[1] were significantly enriched in the set of genes up-regulated in prostate tissues of PB-NICD mice compared to WT mice (57 shared genes, one-sided Fisher's exact test, P = 3.7e-10). Out of 14601 unique genes profiled between the two datasets, 481 were high in our PB-NICD mouse model and 710 were high in the Majumder model (P<0.001 by t-test on log-transformed data, comparing all untreated AKT profiles with untreated WT profiles, using expression dataset GSE3737). Expected shared gene overlap by chance would have been ~24 genes.
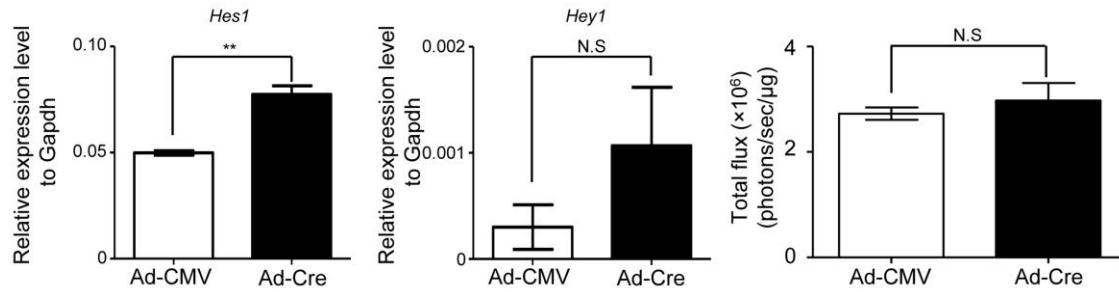
Supplementary Fig. 5: Increased NICD expression does not affect NF-κB activity in basal prostate sphere cells.
Basal prostate sphere cells generated from NICD^{WT}-NFκB-RE bigenic mice were infected with Ad-CMV and Ad-Cre adenovirus separately. QRT-PCR of Hes1 and Hey1 confirmed activation of NICD expression in Ad-Cre infected cells. Bioluminescence imaging showed that NF-κB activity in basal prostate sphere cells was not affected by NICD expression. Data represent means ± s.d. from 2 independent experiments. **: $p < 0.01$ by t-test.
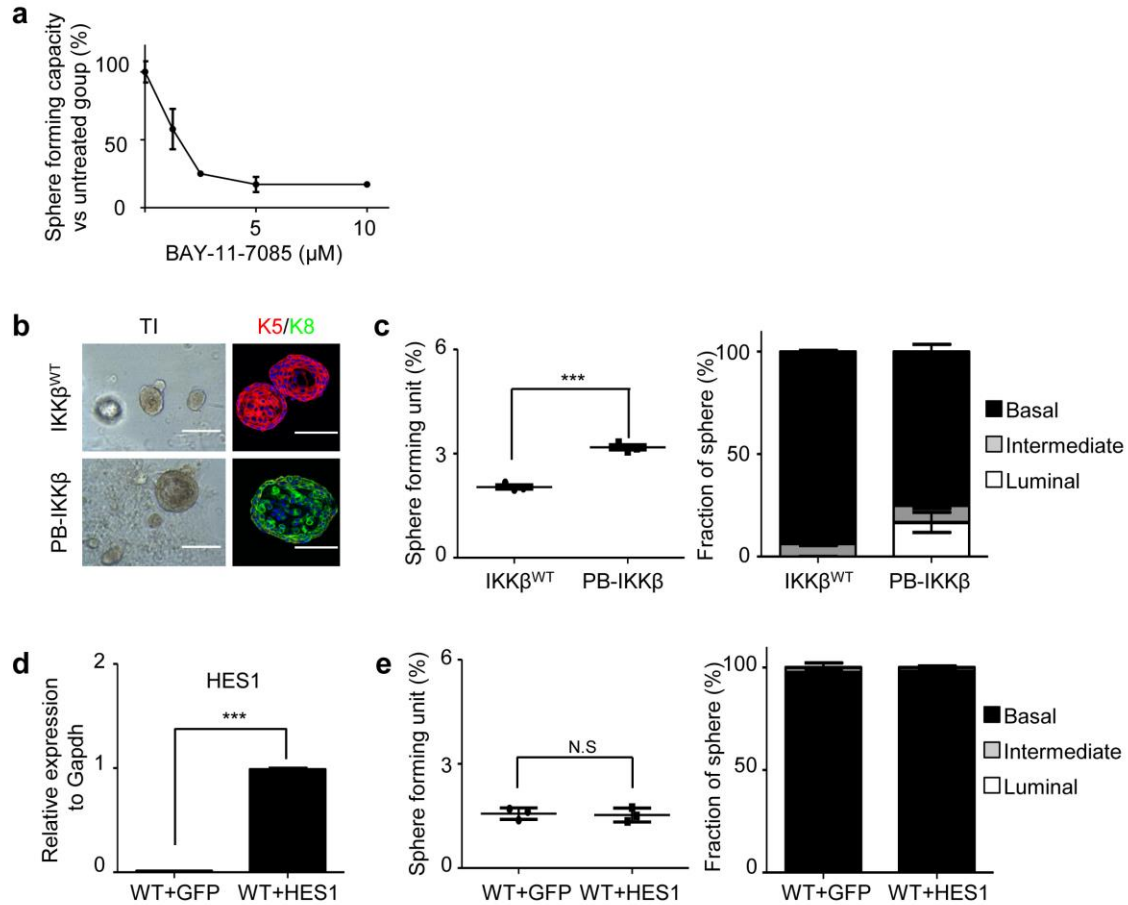
Supplementary Fig. 6: Notch delays anoikis of luminal progenitors by augmenting NF-κB activities independent of Hes1.
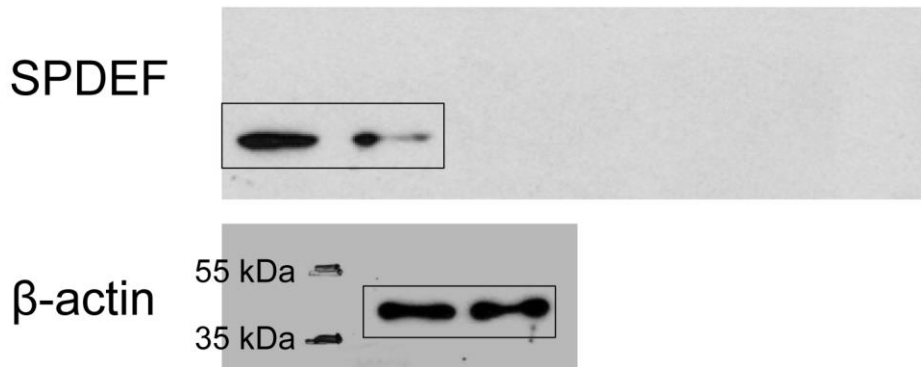
(a) BAY-11-7085 suppresses basal sphere forming activity in a dosage-dependent manner. Data represent means ± s.d. from 3 independent experiments. **(b-c)** Generation of luminal prostate spheres from ARR2PB-Cre;Rosa26-LSL-IKKβ^{ca} (PB-IKKβ) prostate cells. Transillumination (TI) images and IHC analysis of K5 and K8 show the formation of luminal prostate spheres in PB-IKKβ group (b). Dot and bar graphs (c) quantify the sphere-forming units and the types of prostate spheres in IKKβ^{WT} and PB-IKKβ groups. Data represent means ± s.d. from 3 pairs of mice. **(d-e)** Hes1 is not sufficient to drive formation of luminal prostate spheres. QRT-PCR analysis confirms ectopic expression of Hes1 by lentivirus (d). Dot and bar graphs (e) quantify the sphere-forming units and the types of prostate spheres generated from WT prostate cells that have been infected by GFP lentivirus and Hes1 lentivirus separately. Scale bars, 100μm (TI, b); 50μm (K5/K8, b). Data represent means ± s.d. from 3 independent experiments. Statistical significance was calculated using the *t*-test (***: p < 0.001).
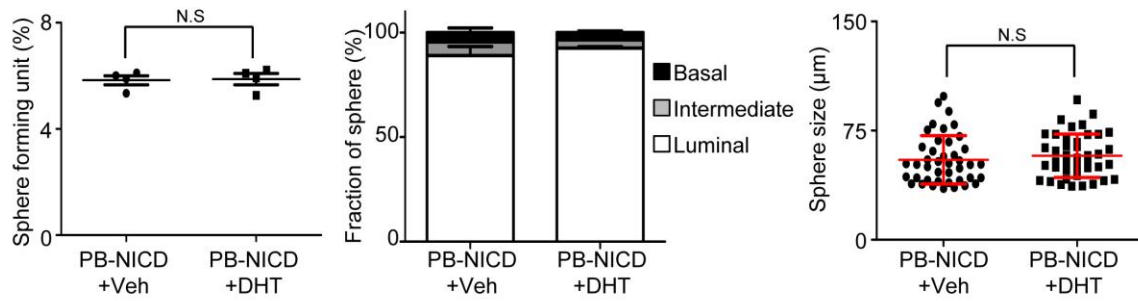
Supplementary Fig. 7: DHT (di-hydro-testosterone) does not affect formation and growth of luminal prostate spheres from PB-NICD cells.
One day after the prostate sphere assay was set up, di-hydro-testosterone was added to a final concentration of 10^{-8} M and replaced every other day. Analyses shown in dot and bar graphs indicate that DHT does not affect sphere forming unit, sphere size or the types of spheres generated. Data represent means ± s.d. from two independent experiments.

Supplementary Figure 8 Unedited full-size blots of Fig. 1

Supplementary Figure 9, Unedited full-size blots of Fig. 4

Total mTOR — 250 kDa

p- mTOR (Ser2448) — 250 kDa

S6 — 35 kDa / 25 kDa

p-S6 (Ser235/Ser236) — 25 kDa

Total 4E-BP1

p-4E-CP1 (Thr37/Thr46)

Total AKT — 70kDa / 55kDa / 35kDa

p- AKT (Ser473) — 70kDa / 55kDa

Total PTEN

β-actin

Full unedited gel for Figure 4b

Total AKT — 70 kDa / 55 kDa

p- AKT (Ser473) — 70 kDa / 55 kDa

β-actin — 55 kDa / 35 kDa

Full unedited gel for Figure 4c
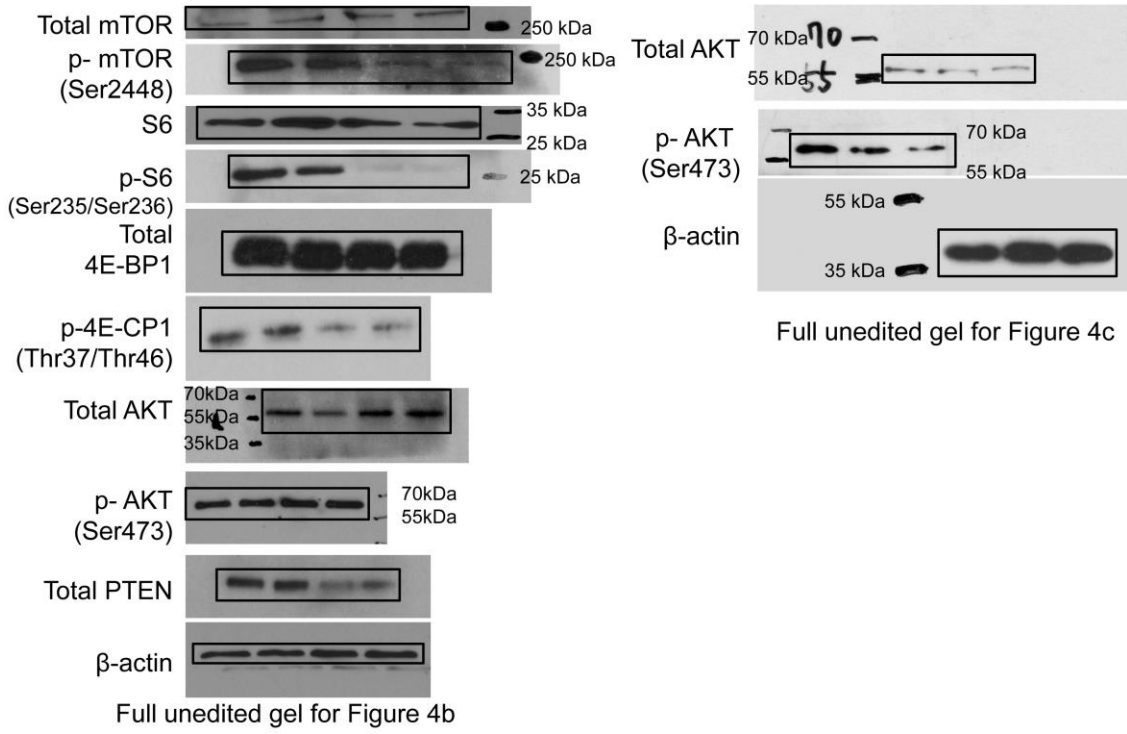
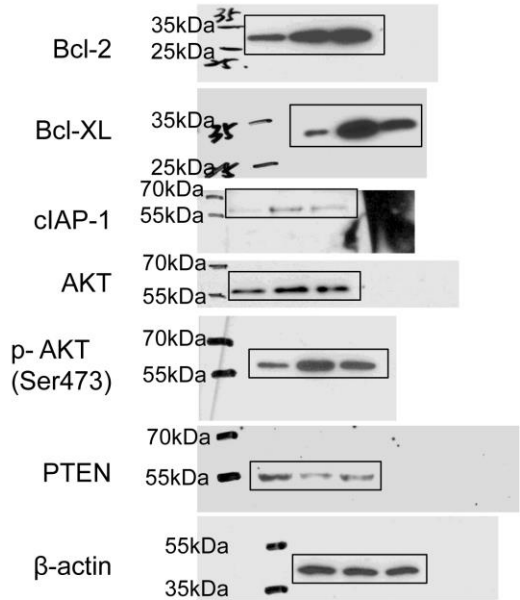**Supplementary Figure 10, Unedited full-size blots of Fig. 5**
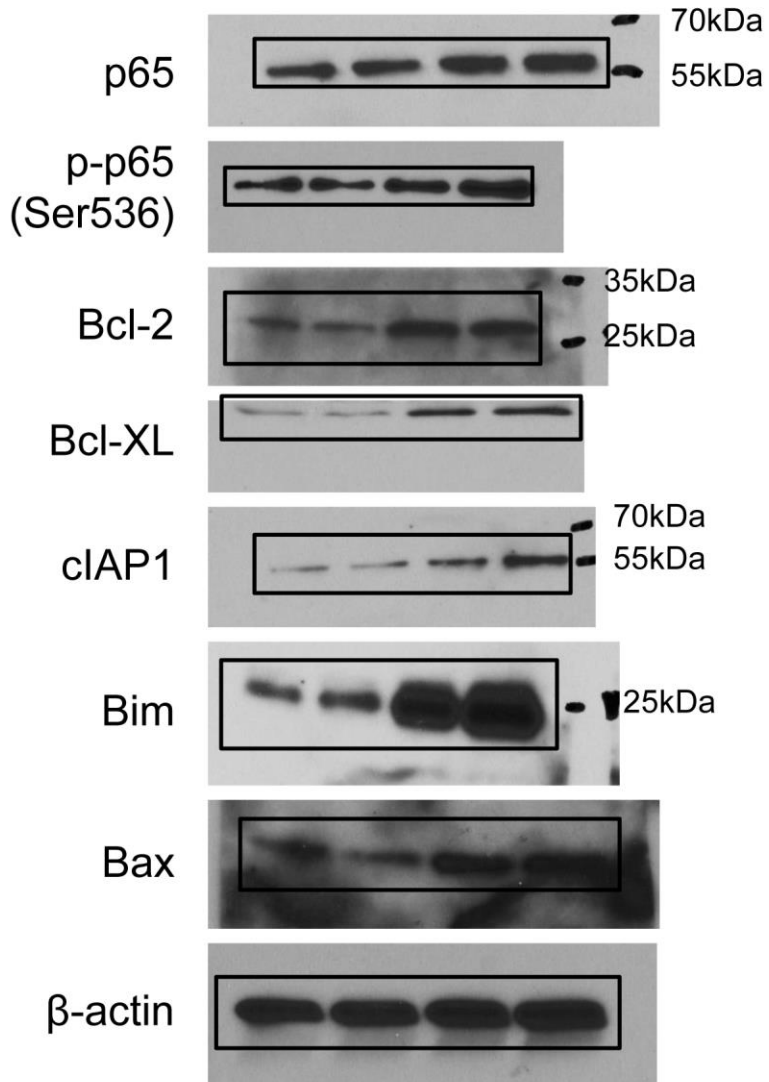
Full unedited gel for Figure 5b

Supplementary Figure 11, Unedited full-size blots of Fig. 6
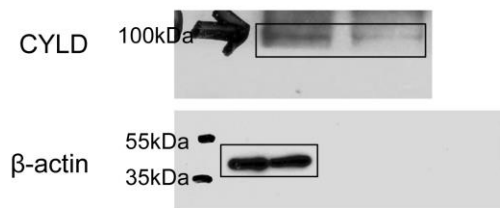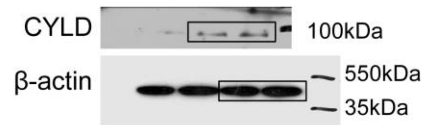
Bcl-2   35kDa 35
         25kDa

Bcl-XL   35kDa 35
         25kDa

cIAP-1   70kDa
         55kDa

AKT   70kDa
         55kDa

p- AKT   70kDa
(Ser473) 55kDa

PTEN   70kDa
         55kDa

β-actin 55kDa
         35kDa

Full unedited gel for Figure 6f,g

CYLD   100kDa

β-actin 55kDa
         35kDa

Full unedited gel for Figure 6h

CYLD   100kDa
β-actin   550kDa
                     35kDa

Full unedited gel for Figure 6i

p- AKT   55kDa
(Ser473) 35kDa

PTEN   55kDa

β-actin

Full unedited gel for Figure 6j

Total AKT   70kDa
            55kDa
            35kDa

p- AKT   70kDa
(Ser473)   55kDa

PTEN   70kDa
            55kDa
            35kDa

β-actin   55kDa
            35kDa
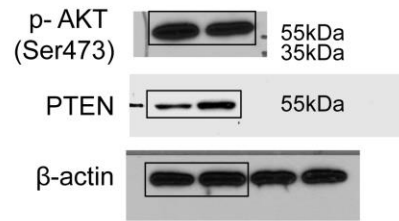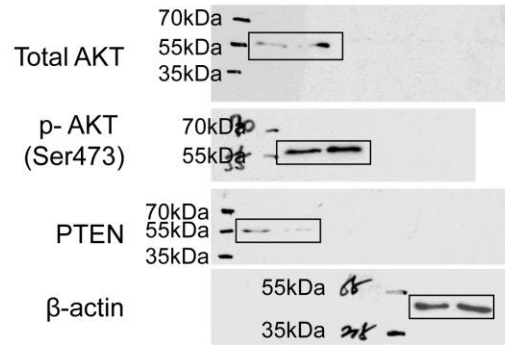
Full unedited gel for Figure 6k

Supplementary Figure 12, Unedited full-size blots of Fig. S3

β-catenin

β-actin
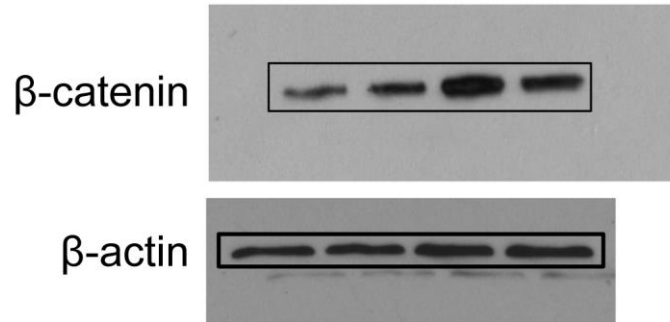
Full unedited gel for Figure S3b

β-catenin

β-actin
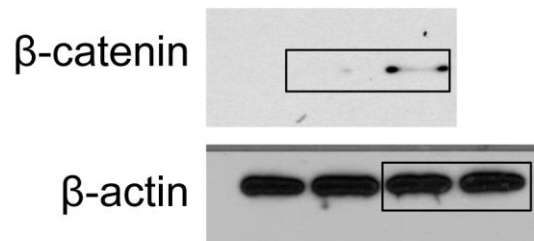
Full unedited gel for Figure S3e

Supplementary Table 1: Mouse genotyping primers

Primers	Sequences (5' to 3')	WT(bp)	TG(bp)
Cre forward	CCTGACAGTGACGGTCCAAAG	None	700
Cre reverse	CATGACTCTTCAACTCAAACT		
RBP-J forward	GAAGGTCGGTTGACACCAGATAGC	250	500
RBP-J reverse 1	ATGTACATTTTGTACTCACAGAGATGGATG		
RBP-J reverse 2	TAATGCACACAAGCATTGTCTGAGTTC		
ICN forward	TAAGCCTGCCCAGAAGACTC	235	320
ICN reverse 1	GAAAGACCGCGAAGAGTTTG		
ICN reverse 2	AAAGTCGCTCTGAGTTGTTAT		
IKKβ forward	WT: CCAGATGACTACCTATCCTC	350	378
	Mut: GCAAGACAGAAGCTTCACGACTC		
IKKβ reverse	WT: GAGCTGCAGTGGAGTAGGCG		
	Mut: GCAATATGGTGGAAAATAAC		
AR$^{fl/Y}$ forward	AGCCTGTATACTCAGTTGGGG	1000	900
AR$^{fl/Y}$ reverse	AATGCAGCATCACATTAAGTTGATACC		
Catnb$^{Lox(ex3)}$ forward	GGTAGGTGAAGCTCAGCGCAGAGC	900	-
Catnb$^{Lox(ex3)}$ reverse	ACGTGTGGCAAGTTCCGCGTCATCC		
NF-κB-RE-Luc f	TGGATTCTAAAACGGATTACCAGGG	-	1000
NF-κB-RE-Luc r	CCAAAACAACAACGGCGGC		

Supplementary Table 2: Mouse qRT-PCR Primers

Primers	Sequences (5' – 3')
Notch1 forward	ACTGTGAGGACGAGGTGGAC
Notch1 reverse	ACAGGCACTCGTTGATCTCC
Hes-1 forward	GGCCTCTGAGCACAGAAAGT
Hes-1 reverse	GAATGCCGGGAGCTATCTTT
Hey1 forward	GGTACCCAGTGCCTTTGAGA
Hey1 reverse	GTGCGCGTCAAAATAACCTT
HeyL forward	GAAGCGCAGCGGGATCATAG
HeyL reverse	CTGTTTCTCAAAGGCAGTGG
CcnD1 forward	GCCCTCCGTATCTTACTTCAAG
CcnD1 reverse	GCGGTCCAGGTAGTTCATG
CcnD2 forward	GCTGTGCATTTACACCGACA
CcnD2 reverse	CCACTTCAGCTTACCCAACA
Bcl-2 forward	AGTACCTGAACCGGCATCTG
Bcl-2 reverse	CATGCTGGGGCCATATAGTT
Bcl2-l1 forward	GTTGGATGGCCACCTATCTG
Bcl2-l1 reverse	GCTGCATTGTTCCCGTAGAG
Tgfa forward	AAGAAGCAAGCCATCACTGC
Tgfa reverse	AGCAGTGGATCAGCACACAG
Egfr forward	TGTGCAAAGGAATTACGACCT
Egfr reverse	GGATTCTCTCCACGGTGTTG
Fgfr2 forward	TGGAGATGATGAGGACGACA
Fgfr2 reverse	CTTCTCGGTGTTGGTCCAGT
AR forward	AATGAGTACCGCATGCACAA
AR reverse	CCCATCCACTGGAATAATGC
Hspa5 forward	AAGGAGACTGCTGAGGCGTA
Hspa5 reverse	TGGGCATCATTGAAGTAAGC
Spink3 forward	CTTTGGCCCTGCTGAGTTTA
Spink3 reverse	CCACTGCATCATGGCAACTA
Pbsn forward	TTCCGTCACATTTGTGTGG
Pbsn reverse	CAGTTGGCACTTAGTCCCTTTC
Prdx6 forward	GAGGATCATCTTGCCTGGAG
Prdx6 reverse	AATGATGGGAAATGGCAACT
Igbp1 forward	GCCTATCCAAATCTCGTTGC
Igbp1 reverse	TGCAGACAACCTATGCTCCA
Azgp1 forward	CCTTGTGACCCTGAAAGACA
Azgp1 reverse	ATCTCGCAACCAAACATTCC
Msmb forward	TGGTGATAGCATCCAAAGCA

Msmb reverse	AGCATCCATGCAGTCATCAG
Car2 forward	GGCTCTGAGCACACTGTGAA
Car2 reverse	GTTGCTGCACAGCTTTTCC
Calr forward	AAGGGCAAGAATGTGCTGAT
Calr reverse	GCCGCACAATCAGTGTGTAT
Sbp forward	GCATGCGGATCTTCTTAAGTG
Sbp reverse	TCTGACCGGGTTCCATAGAC
Fam115e forward	GCCCTTCCCTTTTCAGAGAG
Fam115e reverse	TGGGGTATCCAGAATGAAGG
Pdia3 forward	GCTTGCCCCTGAGTATGAAG
Pdia3 reverse	CAGGTGTTTGTGTTGGCAGT
Spdef forward	GGGCGAGGTCCTGAAAGATA
Spdef reverse	AAAAGCCACTTCTGCACGTT
cMyc forward	AGTGCTGCATGAGGAGACAC
cMyc reverse	GGTTTGCCTCTTCTCCACAG

Supplementary Table 3: Antibodies for IHC and Western blot

Antigen	Supplier	Species	Dilution
K5	Covance #PRB-160P	Rabbit	1:2000
K8	Covance #MMS-162P	Mouse	1:1000
K14	Biogenex MU146-UC	Mouse	1:100
GFP	Clontech, JL8	Mouse	1:1000
P63	Santa Cruz, 4A4	Mouse	1:200
Ki67	Novocastra, NCL-Ki67-P	Rabbit	1:1000
AR	Santa Cruz, sc-816	Rabbit	1:200
NICD	Santa Cruz, sc-6014-R	Rabbit	1:1000
Cleaved caspase3	Cell Signaling, 9661S	Rabbit	1:1000
β-actin	Sigma, A5441	Mouse	1:5000
AKT1	Cell Signaling, 9272	Rabbit	1:1000
phoAKT	Cell Signaling, 4060	Rabbit	1:1000
S6	Cell Signaling, 2217	Rabbit	1:1000
pS6	Cell Signaling, 4857	Rabbit	1:1000
4E-BP1	Cell Signaling, 9644	Rabbit	1:1000
pho4E-BP1	Cell Signaling, 2855	Rabbit	1:1000
mTOR	Cell Signaling, 2983	Rabbit	1:250
phomTOR	Cell Signaling, 5536	Rabbit	1:250
Pten	Cell Signaling, 9559	Rabbit	1:1000
β-catenin	Cell Signaling, 9582	Rabbit	1:1000
Bcl-2	Cell Signaling, 2870	Rabbit	1:1000
Bcl-xL	Cell Signaling, 1764	Rabbit	1:1000
Bim	Cell Signaling, 2933	Rabbit	1:500
Bax	Cell Signaling, 2772	Rabbit	1:500
cIAP1	Cell Signaling, 4952	Rabbit	1:500

Cyld	Cell Signaling, 8462	Rabbit	1:1000
RelA/P65	Cell Signaling, 8242	Rabbit	1:1000
phoRelA/P65	Cell Signaling, 3033	Rabbit	1:1000
α-Mouse	Rockland, IRDye800 610-732-002	Donkey	1:5000
α-Rabbit	Rockland, IRDye700 611-130-002	Goat	1:5000
α-Mouse HRP	Vector Lab. PI-2000	Goat	1:5000
α-Rabbit HRP	Vector Lab. PI-1000	Goat	1:5000

Supplementary references

1. Majumder, P.K.*, et al.* Prostate intraepithelial neoplasia induced by prostate restricted Akt activation: the MPAKT model. *Proc Natl Acad Sci U S A* **100**, 7841-7846 (2003).